Rock and Soil Mechanics

Volume 43 | Issue 7 Article 6

9-20-2022

Buckling failure analysis and numerical manifold method simulation for Malvern Hills slope

Qiu-sheng WANG

Rui-tao ZHANG

Hong ZHENG

Rock and Soil Mechanics 2022 43(7): 1951−1960 ISSN 1000−7598
https: //doi.org/10.16285/j.rsm.2021.6674 rocksoilmech.researchcommons.org/journal

Buckling failure analysis and numerical manifold method simulation for Malvern Hills slope

WANG Qiu-sheng, ZHANG Rui-tao, ZHENG Hong

The Key Laboratory of Urban Security and Disaster Engineering of Ministry of Education, Beijing University of Technology, Beijing 100124, China

Abstract: Based on the energy equilibrium, the computational formula of critical buckling length of multi-layer rock slope is derived. Considering interlayer and cross joints, the numerical manifold method is used to simulate the buckling evolution process of Malvern hills slope in New Zealand, and the theoretical calculation and numerical simulation results are compared with the field measured data. The results show that numerical manifold method can accurately simulate slope buckling failure process by preforming interlayer and cross joints. The process of slope buckling deformation and instability failure can be divided into interlayer dislocation-slight bending, slope toe traction-sharp uplift and accelerated sliding-landslide formation. Under the long-term action of self-weight, the evolution of slope buckling from formation to failure mainly includes three stages: initial bending, sharp bending and landslide formation. The angle between cross joint and slope normal is defined as β. Among the four kinds of cross joints with the angle β of 0°, 15°, 30° and 45°, the slope with 45° cross joint is most prone to slipping and bending deformation, the degree of buckling is the largest, and the number of time steps of slipping and bending is the least. When β is in the range of 30°–45°, the numerical simulation results are in good agreement with the reality.

Keywords: layered slope; buckling failure; numerical manifold method; cross joint

1 Introduction

Buckling is one of the typical failure modes of landslide. Under the long-term action of self-weight, the rock layers at the top of the slope slides and at the toe of the slope are blocked, resulting in the uplift deformation and failure of rock layers. Slope buckling is usually developed in the deep canyon, resulting in large-scale landslides and causing serious harm to the safety of human life and property, such as Lijiaxia landslide [1] in the upper reaches of the Yellow River, Bawangshan landslide [2] in Ertan Hydropower Station, Malvern Hills [3] in New Zealand, and Westfield open pit coal mine [4] in the United States. The study on the formation and failure mechanism of layered rock slope buckling can provide a reliable basis for the prevention and control of buckling landslide and is of great significance to the safety of human life and property.

Sun [5] and Goodman [6] analyzed the slope buckling by using the pressure bar stability theory. Liu et al.[7], Zhu et al.[8] and Feng et al.[9] established a mechanical criterion of single-layer slope buckling failure by using the energy method based elastic plate and elastic-plastic plate theory. In addition, many scholars have studied the formation mechanism of slope buckling failure by employing physical and mechanical models[10−12]. However, due to the limitations of the test space, the physical model is different from the actual slope, and most of the model tests only consider the rock layer joints and do not consider the cross joints intersecting with the rock layer.

With the development of computer technology, finite element method (FEM), discrete element method (DEM) and discontinuous deformation analysis (DDA) have been widely used in the analyses of slope buckling and instability. Pant et al.[13] and Adhikary et al.[14] studied the bending and buckling mechanism of foliated rock slope based on the large deformation Cosserat continuum model. Pereira et al.[15] and Silva et al.[16] simulated the buckling failure process of phyllite slope with finite element software Phase2 and studied the influence of structural plane stiffness, cohesion, and in-situ stress on the buckling failure mechanism of the slope. In the scheme of FEM, the slope is processed as a continuum body, and the stress and deformation before the buckling failure can be easily obtained. However, it is difficult to address the discontinuities such as cracks and the deformation after the structural failure.

Tommasi et al.[17] used DEM and DDA methods to simulate the three-hinge buckling failure of Lavini di Marco slope, examined the influence of rock mass characteristics, slope geometry, and water pressure on

Received: 4 October 2021 Revised: 28 March 2022
This work was supported by the Key Project of National Natural Science Foundation of China (52130905) and the National Key Research and Development Project of China (2018YFC1505001).
First author: WANG Qius-heng, male, born in 1977, PhD, Professor, research interests: deformation and failure of underground engineering. E-mail: wangqs@bjut.edu.cn

slope buckling, and concluded that the slope would be subject to buckling deformation under the conditions of high water pressure and large-scale small deflection. Tang et al. [12] employed DEM software to simulate the sliding and bending process of the layered slope. Combined with the physical model and theoretical calculation, they investigated the mutual restriction and influence among the dip angle, single layer thickness, critical slope length, and buckling depth, and proposed the geomechanical conditions, critical buckling state discrimination and early identification marks for the sliding and bending deformation of the layered slope. Based on discontinuity mechanics, the rock structure is processed as discrete blocks in DEM and DDA, and the blocks are connected by contact bounds. They are suitable for simulating the movement of blocks and the contact between discontinuities in the rock structure. However, no matter the size of the blocks, each block is taken as an element in the simulation. It is still difficult to simulate the deformation of discontinuous structures with defects and cracks. Consequently, it is difficult to obtain ideal results by employing the two methods for the actual slope buckling failure.

The numerical manifold method is a new numerical method that integrates the continuous and discontinuous methods[18] and can be used to study the movement of rock slopes with continuous and discontinuous deformation. Although the numerical manifold method has been widely used to simulate structural failure and deformation [19−25], the research on the formation and failure process of multi-layer rock slopes by the numerical manifold method is seldom reported. Currently, most of the research on the influencing factors of slope buckling failure are the geometric dimensions such as slope length, slope angle and rock layer thickness, and less attention is paid to the cross joints of lateral structural planes of rock layers. In this paper, a formula for calculating the critical buckling length of multi-layer rock slope is derived based on the principle of energy method. Considering the interlayer and cross joints, the numerical manifold method is used to simulate the formation and failure process of Malvern Hills slope buckling, and the influence of cross joints of rock layers on slope buckling and failure is investigated.

2 Theoretical calculation of critical buckling length

It is assumed that there is a soft interlayer, namely a sliding surface between the rock layers. The rock layer slides and bends only along the sliding surface. The rock layer cannot be compressed during the sliding, and the rock layer below the sliding surface does not slide, as shown in Fig. 1. According to the literature[5−6], the rock layer in the bending section is simplified as a beam and analyzed with the pressure bar stability theory. The mechanical calculation model of the layered slope is shown in Fig. 2, where G is the gravity of the rock layer and F is the residual sliding force of the rock layer. Assuming that the slope length is L and the length of the buckling section is l_0, then the length of sliding part is $L–l_0$. The unit weight of rock layer is γ, the single layer thickness is D, the number of layers is n, and the slope angle is θ, the cohesion between rock layers is c and the internal friction angle is φ. If the unit width of rock layer is taken, the residual force F can be expressed as

$$F = n\gamma d\left(L - l_0\right)\left(\sin\theta - \cos\theta \cdot \tan\varphi\right) - \left(L - l_0\right)c \quad (1)$$

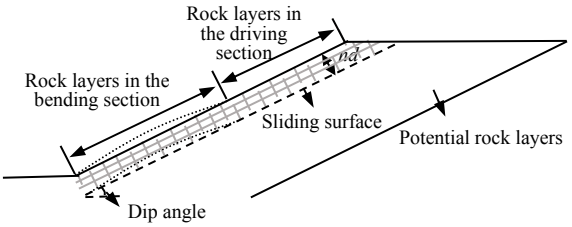

Fig. 1 Bucking failure model of layered rock slope

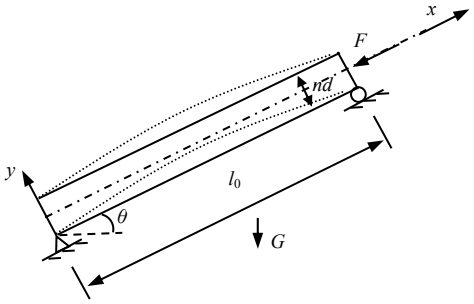

Fig. 2 Mechanical calculation model of slope

Assuming that the deflection of each rock layer in the bending section is the same, and the maximum deflection is δ, the deflection deformation curve of each rock layer can be expressed as

$$y = \delta \sin\left(\frac{\pi}{l_0}x\right) \quad (2)$$

Ignoring the axial compression deformation of rock layer, the sliding displacement driven by the residual force F can be calculated with the following formula:

$$y\left(l_0\right) = \int_0^{l_0} \mathrm{d}s - l_0 = \int_0^{l_0}\left(\sqrt{1+\left(y'\right)^2} - 1\right)\mathrm{d}x = \frac{\pi^2\delta^2}{4l_0} \quad (3)$$

where $\mathrm{d}s$ is the arc differential of the bending section.

The sum of the work done by the residual sliding force and the gravity component along the slope of the

rock layer in the bending section is equal to the sum of the elastic energy stored in the bending section and the work done by the gravity component perpendicular to the slope of the rock layer in the bending section, which can be expressed as

$$W_F + W_{G//} = W_{G\perp} + W_S \tag{4}$$

where W_F is the work done by the residual sliding force; $W_{G//}$ is the work done by the gravity component of the rock layer along the slope in the bending section; $W_{G\perp}$ is the work done by the gravity component of the rock layer perpendicular to the slope in the bending section; and W_S is the elastic energy stored in the bending section. The calculation formula is as follows:

$$W_F = F \cdot y(l_0) = \frac{\pi^2\delta^2}{4l_0}\left[n\gamma d(L-l_0)(\sin\theta - \cos\theta\cdot\tan\varphi) - (L-l_0)c\right] \tag{5}$$

$$W_{G//} = \frac{1}{2}\int_0^{l_0}\left(n\gamma d\sin\theta\cdot\int_0^x (y')^2\,\mathrm{d}x\right)\mathrm{d}x = \frac{\pi^2\delta^2 n\gamma d\sin\theta}{8} \tag{6}$$

$$W_{G\perp} = \int_0^{l_0}(n\gamma db\cos\theta\cdot y)\,\mathrm{d}x = \frac{2\delta n\gamma d l_0\cos\theta}{\pi} \tag{7}$$

$$W_S = \frac{1}{2}\int_0^{l_0}\left(\sum_{i=1}^{n} E_i I_i\cdot(y'')^2\right)\mathrm{d}x = \frac{n\delta^2\pi^4 EI}{4l_0^3} \tag{8}$$

Where E is the elastic modulus of rock; I is the inertia moment of single layer rock.

Substituting Eqs. (5)−(8) into Eq. (4) gives

$$\begin{aligned}&(-n\gamma d\sin\theta + 2n\gamma d\cos\theta\tan\varphi + 2c)\delta\pi^3 l_0^3 + \\ &2(n\gamma d\sin\theta - n\gamma d\cos\theta\tan\varphi - c)\delta\pi^3 L l_0^2 - \\ &\frac{nE\delta\pi^5 d^3}{6} - 16n\gamma d l_0^4\cos\theta = 0\end{aligned} \tag{9}$$

Performing the partial derivative on both sides of Eq. (9), the univariate cubic equation with respect to the critical buckling length l_0 can be obtained:

$$l_0^3 + k_1 l_0^2 - k_2 = 0 \tag{10}$$

where

$$\left.\begin{aligned}k_1 &= \frac{2L(n\gamma d\sin\theta - n\gamma d\cos\theta\tan\varphi - c)}{-n\gamma d\sin\theta + 2n\gamma d\cos\theta\tan\varphi + 2c} \\ k_2 &= \frac{nE\pi^2 d^3}{6(-n\gamma d\sin\theta + 2n\gamma d\cos\theta\tan\varphi + 2c)(1-v^2)}\end{aligned}\right\} \tag{11}$$

where v is the Poisson's ratio of rock.

For any layered slope with the given parameters listed above, the critical buckling length of the slope can be obtained by solving Eq. (10). The ratio of the critical buckling length l_0 to the total length of the slope L is defined as the slope stability coefficient λ:

$$\lambda = \frac{l_0}{L} \tag{12}$$

That is, when $0 < \lambda < 1$, buckling failure will happen; and if $\lambda > 1$, the slope is stable.

3 Numerical simulation

3.1 Local displacement and global displacement

In the numerical manifold method, the physical element can be arbitrary polygon. The local displacement field of a physical element is approximated by a polynomial or analytic displacement function, and the global displacement approximation of the material is obtained by summing the weighted average values of local approximation of all physical elements. Assuming that the material is covered by m physical patches, the global displacement approximation can be expressed as

$$U(z) = \sum_{i=1}^{m}\omega_i(z)\cdot u_i(z) \tag{13}$$

where z indicates arbitrary point in the material; $\omega_i(z)$ is the weight function of the i-th physical patch; $u_i(z)$ is the local displacement approximation on the i-th physical patch.

The three-node triangular element based mathematical cover is used to study the buckling failure of rock slope. Each manifold element is covered by three physical patches, and the weight function of each physical patch can be expressed in area coordinates:

$$\omega_i = L_i = \frac{a_i + b_i x + c_i y}{2A} \tag{14}$$

where (x, y) is the coordinate of any point in the element; A is the area of triangular element; a_i, b_i and c_i are the coefficients to be determined, i = 1, 2, 3.

For the two-dimensional manifold method, each physical element or node displacement contains two unknowns, i.e., horizontal x-direction displacement and vertical y-direction displacement. According to the principle of minimum potential energy, the overall equilibrium equation of m physical elements can be obtained:

$$\boldsymbol{K}_{m\times m}\cdot\boldsymbol{D}_{m\times 1} = \boldsymbol{F}_{m\times 1} \tag{15}$$

where $\boldsymbol{K}_{m\times m}$ is the stiffness matrix; $\boldsymbol{D}_{m\times 1}$ is the node displacement vector; and $\boldsymbol{F}_{m\times 1}$ is the load vector.

3.2 Large deformation and contact simulation

The numerical manifold method adopts the block motion theory in DDA to simulate the large deformation movement problem. By applying and removing the spring on the contact boundary, the open and close

iteration is realized, so that there is no tension and embedding between the blocks in the movement process. There are three states at the boundary between blocks, namely, opening, locking, and sliding. By exerting normal and tangential springs, the boundary contact states open-to-lock and slide-to-lock can be realized, respectively. When sliding between boundaries, the friction force is applied to modify the stiffness matrix, and the calculated boundary contact force is added into the equilibrium force array and delivered to the next iteration [18].

Shi[18] put forward a strict contact detection method in DDA. By using this method, contact forms such as corner to edge, edge to edge, convex corner to convex corner, and convex corner to concave corner can be obtained. The connection of discontinuities is achieved by applying normal and tangential stiffness springs on the contact boundaries. The normal and tangential stiffness can be calculated as follows:

$$K_{\mathrm{n}}=\frac{\mu_1 El}{2} \tag{16}$$

$$K_{\tau}=\frac{G'l}{2}=\frac{\mu_2 El}{2} \tag{17}$$

where E and G' are the elastic modulus and shear modulus of the material, respectively; μ_1 and μ_2 are contact stiffness enhancement coefficients, which can be determined according to trial calculation; and l is the length of the contact surface.

3.3 Rock strength reduction

The elastic modulus of rock is an important parameter for slope stability analysis. However, after long-term weathering, erosion, and other physical and chemical actions, the rock layer of the slope will be fractured, and its strength is smaller than that of the intact rock. Therefore, it is necessary to reduce the elastic modulus of the rock of slope in consideration of the geological strength index. According to Hoek-Diederichs model[26], the reduced elastic modulus can be estimated according to the following formula:

$$E_{\mathrm{m}}=E\left\{0.02+\frac{1-0.5D}{1+\exp\left[\left(60+15D-\mathrm{GSI}\right)/11\right]}\right\} \tag{18}$$

where GSI is the geological strength index, which is divided by rock type; D is the factor reflecting the disturbance degree of rock mass, for the natural slope, 0 is suggested.

Tensile strength is an important index reflecting the physical and mechanical properties of rock. Reliable rock strength evaluation is of great significance to the stability analysis of layered rock slope. In addition, the rock classification and the rock disturbance degree also have an impact on its strength. Therefore, in order to obtain effective rock strength, Hoek-Brown criterion is adopted to estimate the tensile strength of slope rock[27−28]. The calculation formulas are as follows:

$$\sigma_{\mathrm{tm}}=\frac{\sigma_{\mathrm{c}}}{2}\left(m_{\mathrm{b}}-\sqrt{m_{\mathrm{b}}^2+4s}\right) \tag{19}$$

$$m_{\mathrm{b}}=m_{\mathrm{i}}\exp\left(\frac{\mathrm{GSI}-100}{28-14D}\right) \tag{20}$$

$$s=\exp\left(\frac{\mathrm{GSI}-100}{9-3D}\right) \tag{21}$$

where σ_{tm} is the tensile strength of rock; σ_{c} is the compressive strength of rock; m_{i} is a material constant, which depends on the crystal structure and grain size of the rock; m_{b} and s are predefined parameters.

4 Case study

4.1 Slope condition

The buckling phenomenon of the natural slope and artificial slope is often found after buckling failure. It is difficult to measure the critical buckling length of the slope, which brings challenges to numerical simulation. Malvern Hills is an opencast coal mine located in Canterbury, inland New Zealand[3]. July 1, 2004, the rock layer of the slope slipped along the slope, and buckling failure occurred at the toe of the slope. From the damage site, the sliding trace at the slope top and the folded rock layer at the slope toe were clearly seen. The actual buckling length of the slope was estimated by the measured sliding displacement at the slope top, which can be compared with the numerical analysis. Therefore, this paper takes Malvern Hills as an example to study the failure mechanism of slope buckling. As shown in Fig. 3, the slope angle is about 42°, the slope height is 15 m, and the lateral extension is 85 m. The total thickness of the rock layer in the buckling section is about 2 m, and the unit weight is 22 kN/m^3. The rock layer at the top of slope slides downward by 6.2 m (the vertical displacement is about 4.2 m). The rock layer at the toe of the slope folds and forms a pile, covering the 355RL platform, of which the horizontal width is 5 m. The rock of the slope is mudstone, and the color is gray white and gray black. The average distance between the interlayer joints is about 0.2 m. There are also joints in the vertical direction of the rock layers, and the joints are separated by 3 cm wide argillaceous fissures[3]. According to literature[3, 27−29], the uniaxial compressive strength σ_{c}, elastic modulus E, Poisson's ratio v, mechanical parameters of sliding surface, GSI, rock disturbance degree D, and rock material constant m_{i} of the slope are shown in Table 1.

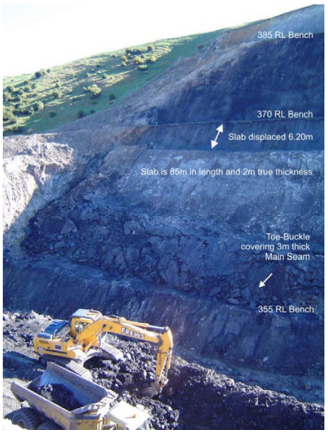

Fig. 3 Bucking failure characteristics of Malvern Hills slope[3]

Table 1 Physical and mechanical parameters of slope rock and strata

Material	σ_c/MPa	E/GPa	v	φ/(°)	c/kPa	GSI	D	m_i
Rock/Rock layer	25	0.61	0.3	3−25	0	35	0.7	9

4.2 Calculational model

According to the actual conditions of the slope, during the buckling failure, only the 355RL platform at the slope toe has an obstruction effect on the sliding rock layers. The rock layers at 370RL platform and 385RL platform at the upper end of the slope don't slide and have no impact on the sliding rock layers in the buckling section. Therefore, during the modeling, only 355RL platform is considered. The two-dimensional calculation model established with O as the origin is shown in Fig. 4, where $BCGH$ corresponds to a layered slope with a thickness of 2 m. The slope height is 15 m. The spacing for the joints parallel to the slope is 0.2 m, and 10 layers in total. The spacing for the joints perpendicular to the slope is 0.5 m. GH indicates a weak interlayer, and CD corresponds to 355RL platform. The $GAFEDCH$ boundary is set as fixed constraint. P is the displacement monitoring point at the top of the slope, and K1−K6 are the displacement monitoring points at the buckling section. Rotate the vertical joint anticlockwise and change the angle between it and the normal vector of the slope, set the intersection angles as 0°, 15°, 30°, and 45°, respectively, as shown in Fig. 5, and observe the formation and failure process of slope buckling under different intersection angles.

The three-node triangular element is used for the numerical manifold cover. According to the rock strength reduction principle mentioned in the previous section, the elastic modulus E_m of the slope rock is taken as 0.027 GPA, and the tensile strength is taken as 8 kPa, and the other parameters remain unchanged. The number of calculation time steps is set to 5 000, and the maximum displacement ratio in each step is 0.001. The time step is set as 0.001 s. The dynamic coefficient is 1.0. The overrelaxation iteration coefficient is 1.8, and the contact spring stiffness is 0.027 GPa. Taking the vertical inclined joint β=0 ° as an example, the mathematical cover and physical cover are shown in Fig. 6. A total of 806 manifold elements are generated, and each manifold element is covered by 3 physical patches.

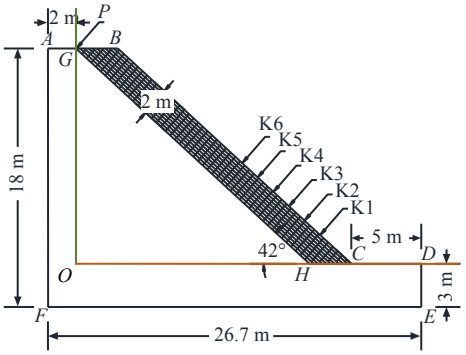

Fig. 4 Calculation model of Malvern Hills slope

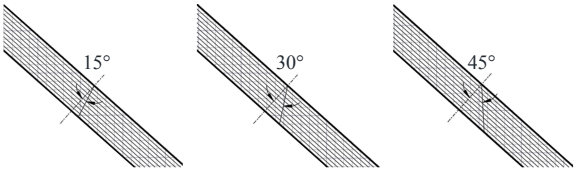

(a) β=15° joint (b) β=30° joint (c) β=45° joint

Fig. 5 Schematic diagrams of different cross joints

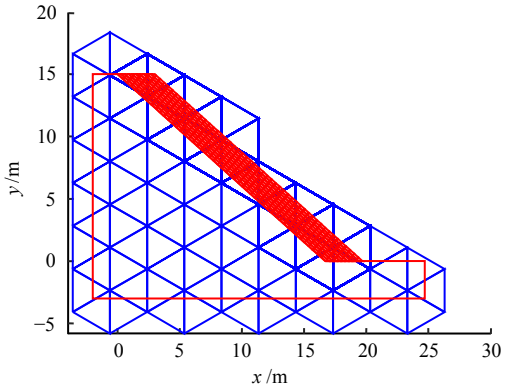

(a) Mathematical cover

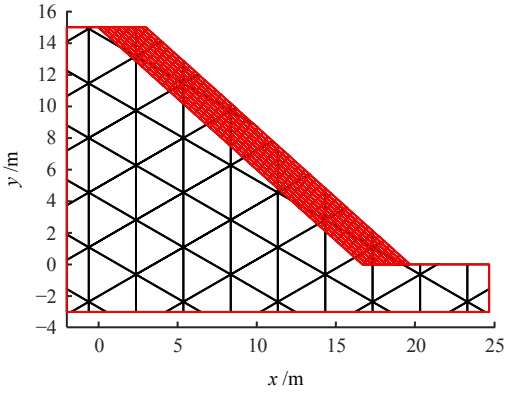

(b) Physical cover

Fig. 6 Numerical manifold model

5 Simulation result and analysis

5.1 Failure characteristics of slope buckling

The failure characteristics of slope buckling under different cross joints are shown in Fig. 7. It can be seen from Fig. 7 that the dip angle β of the cross joint has a great influence on the buckling deformation of the slope. When the joint inclination $\beta = 0°$, the rock layers at the top of the slope will slide downward slightly, and the rock layers at the foot of the slope do not swell, and the slope tends to be stable. When the joint dip angle is 15°, there is no obvious deformation of the slope when the time step is 1 000, and when the time step is 3 000, there is a sliding displacement at the slope top and a slight deformation near the slope toe, and when the time step is 5 000, the sliding displacement at the slope top increases, but the slope still tends to be

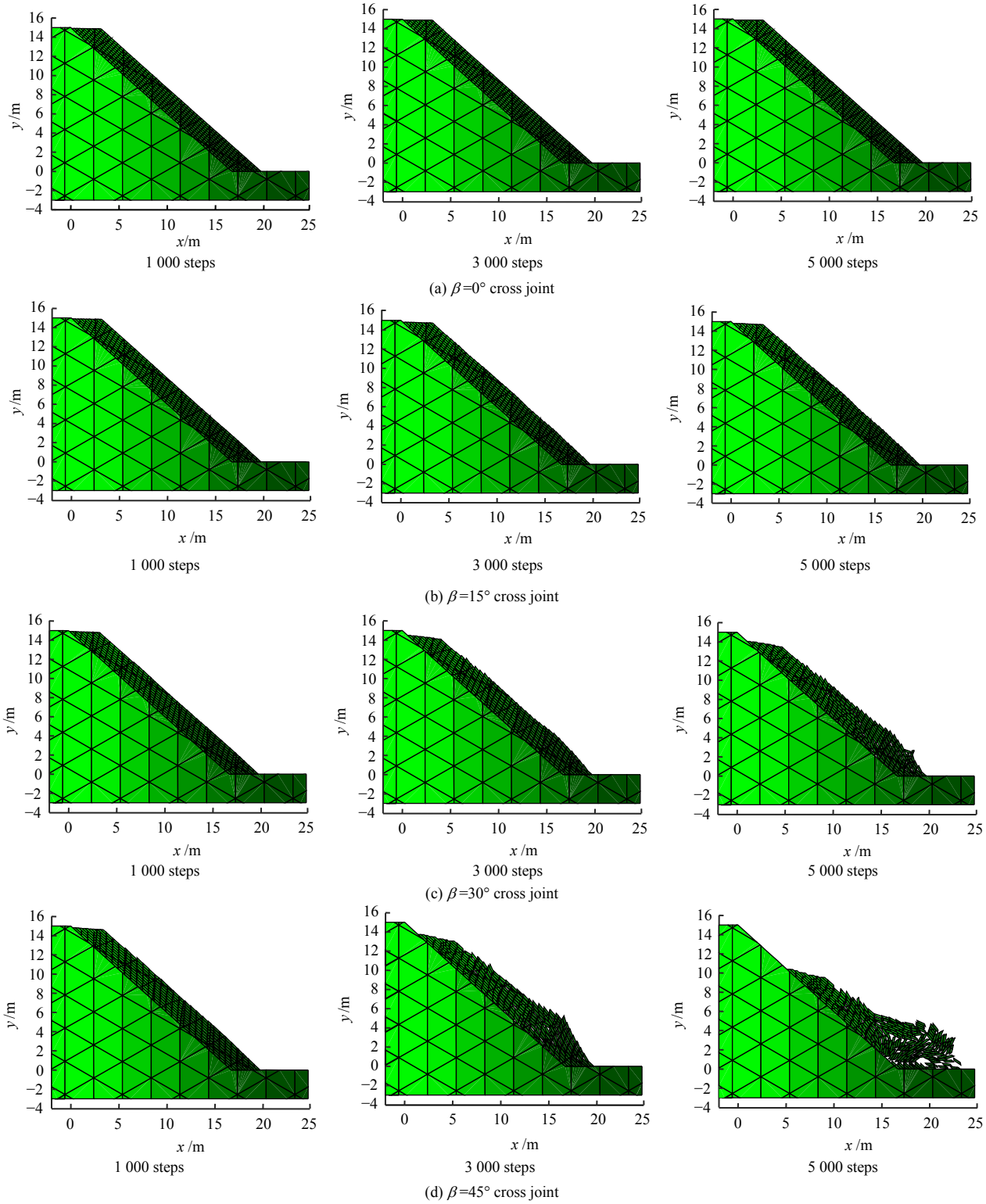

Fig. 7 Bucking failure characteristics of slopes with different cross joints

https://rocksoilmech.researchcommons.org/journal/vol43/iss7/6
DOI: 10.16285/j.rsm.2021.6674

stable. When the joint dip angle is 30°, the rock layers at the top of the slope slide slightly at 1 000 steps. At 3 000 steps, the rock layers at the top of the slope slide significantly, and the rock layers at the foot of the slope bend slightly. At 5 000 steps, the sliding displacement of the rock layers at the top of the slope increases, and the uplift deformation of the rock layers near the foot of the slope increases sharply, resulting in local delamination. When the joint dip angle is 45°, the rock layers at the slope top slide and near the slope toe slide slightly at 1 000 steps. At 3 000 steps, the rock layers at the slope top slide significantly and the differential dislocation appears, and the uplift deformation of the rock layers near the slope toe increases sharply. At 5 000 steps, the rock layers in the bending section of the slope are seriously damaged, and landslide occurs, and finally, a deposit is formed at the foot of the slope. According to the above analysis, the characteristics of slope buckling deformation and instability failure can be divided into interlayer dislocation-slight bending, slope toe traction-sharp uplift and accelerated sliding-landslide formation.

5.2 Slope displacement and critical buckling length

Figures 8 and 9 show the vertical displacement contours of the slopes with different cross joints and the vertical displacement variation curves of monitoring point *P* at the slope top. As displayed in Figs. 8 and 9, when the dip angles of cross joint β are 0° and 15°, there is slight sliding at the top of the slope and no obvious uplift deformation of the rock layers near the slope toe. After sliding a certain distance at the slop top, the slope tends to be stable. When the dip angles of cross joint β are 30° and 45°, the sliding displacement at the slope top gradually increases with the increase of the time step. When β is 30°, the sliding speed of the slope is relatively slow, and the rock layers near the slope toe uplift obviously at 5 000 steps. When β is 45 °, the sliding speed at the slope top is slow at the initial stage and starts to accelerate around 3 500 steps, and the slope has undergone severe deformation and gradually forms a landslide at 5 000 steps. Through the above analysis, it can be seen that when β is 45°, the bending deformation of the rock layers is the fastest, and the number of time steps of slipping and bending is the least. With the development of bending deformation layer by layer, the uplift degree of the rock layers near the slope toe reaches the maximum. Subsequently, the resistance of the rock layers below the highest position of the slope uplift to the upper rock layers gradually decreases, and the sliding speed at the slope top is accelerated, and finally, a landslide is formed. In addition, the critical buckling length of the slope can be estimated according to the displacement

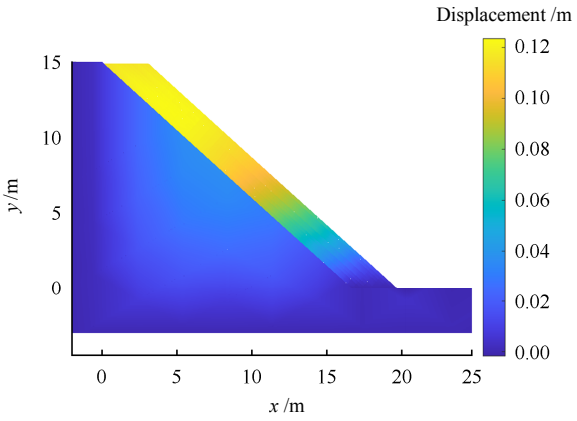

(a) β=0° vertical displacement contour

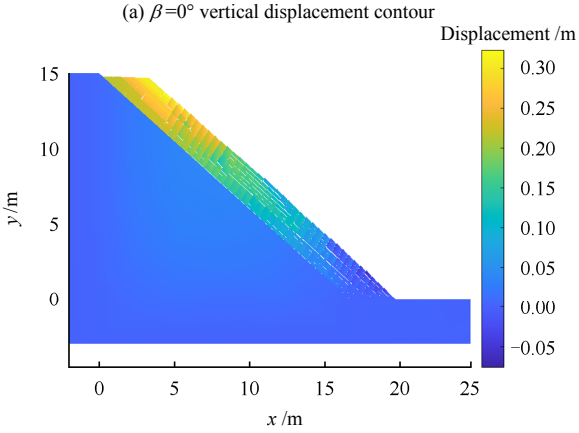

(b) β=15° vertical displacement contour

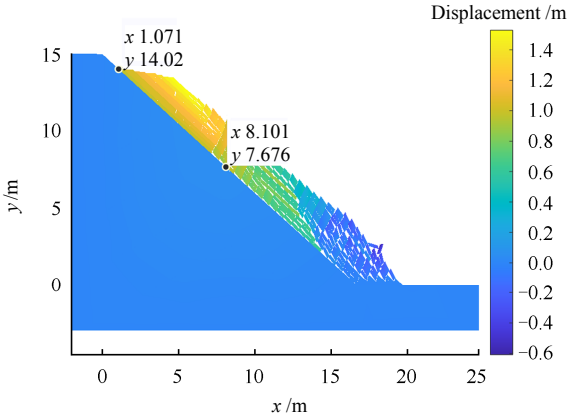

(c) β=30° vertical displacement contour

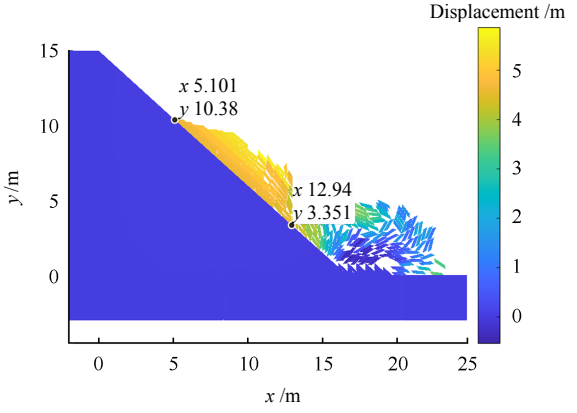

(d) β=45°vertical displacement contour

Fig. 8 Vertical displacement contours of buckling slopes with different cross joints

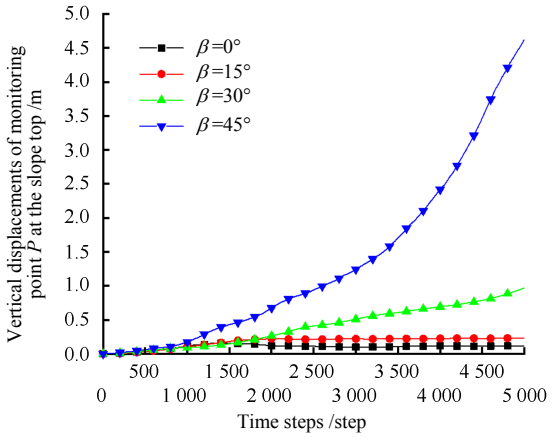

Fig. 9 Vertical displacements of monitoring point *P* at the top of slope with different cross joints

contour. The range of the whole slope rock layers L can be divided into a buckling section l_0 and a sliding section $L-l_0$. The sliding displacement of each rock layer in the sliding section is equal, which indicates that the corresponding colors of the rock layers in the sliding section are the same or similar on the displacement contour. The coordinates of the start point M_1 and the end point M_2 of the sliding section can be obtained according to the displacement contour. The coordinates of the two points have been marked in Figs. 8(c) and 8(d), then the length of the sliding section can be obtained, and then the critical buckling section length l_0 can be obtained:

$$l_0 = L - \sqrt{(x_1 - x_2)^2 + (y_1 - y_2)^2} \quad (22)$$

where (x_1, y_1) and (x_2, y_2) are M_1 and M_2 coordinates, respectively.

Figure 10(a) shows the horizontal displacement variation curves of monitoring points in the buckling section. In the period of 0−3 500 steps, the horizontal displacement of each monitoring point gradually increases with the increase of the time step, but the growth rate is slow. After 3 500 steps, the growth rate of horizontal displacement of each monitoring point increases gradually, of which the displacements of monitoring points K3 and K4 are the largest and the growth rates are the fastest. This indicates that the maximum position of slope bending and buckling uplift is between K3 and K4. Fig.10(b) shows the vertical displacement variation curves of the monitoring points in the buckling section. It is specified that the downward sliding is positive. It can be observed from Fig. 10(b) that when the time step is between 0 and 500, the monitoring points K1−K4 move downward slowly, and at 500 steps, the monitoring points K1−K4 start to move upward gradually, namely the rock layers start to generate uplift deformation, and the maximum uplift displacement is reached around 3 500 steps. The displacement value of the monitoring point K3 is the largest. Then the monitoring points K1−K4 start to move downward and accelerate, and the downward speed of K3 monitoring point is the fastest and the displacement value is the largest. On the contrary, monitoring points K5 and K6 move downward with the increase of time step. Before step 3 500, the displacement of monitoring point K6 increases slowly, and after step 3 500, it begins to move downward rapidly. The displacement of monitoring point K5 changes little from step 0 to step 4 000, and after step 4 000, it begins to move downward rapidly. To sum up, according to the horizontal and vertical displacement change laws of each monitoring point, it can be concluded that step 3 500 is the critical node of slope buckling failure, the corresponding rock layers reach the maximum degree of buckling, and the maximum uplift position is near monitoring point K3, which is about 0.75 m higher than the initial position. In combination with the displacement contours in Figs. 8(c) and 8(d), it can also be confirmed that the location of the maximum slope buckling uplift is in the vicinity of monitoring point K3 (see Fig. 4 for the distribution of monitoring points K1−K6).

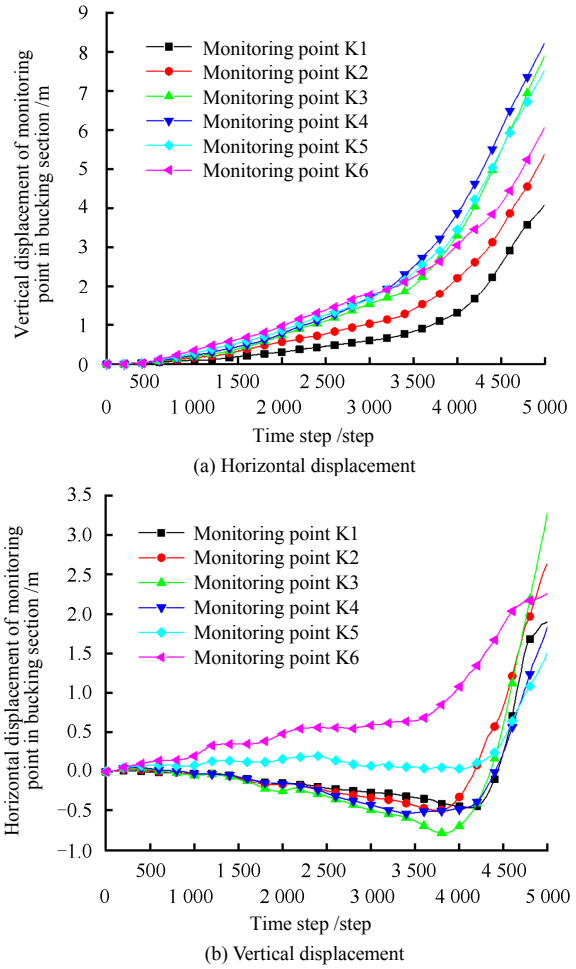

Fig. 10 Horizontal and vertical displacements of monitoring points in bucking section

6 Discussion

Slope buckling is the result of long-term deformation evolution of rock layers under the action of self-weight, and the buckling failure is the gradual evolution process from buckling to landslide. Comparing the numerical simulation results (see Figs. 7 and 8) with the actual slope failure characteristics (see Fig. 3), it can be seen that in the range of 0°−45°, with the increase of the dip angle of cross joint, the better effect of buckling failure can be simulated by the numerical manifold method, and the simulated results of the slope buckling failure characteristics (Figs.7 (c) and 7 (d)) are consistent with the actual situation. When the dip angle of cross joint is between 0° and 1 °, the rock layers at the top of the slope slide slightly, but no obvious uplift deformation in the lower rock layers, and the slope tends to be stable. When the dip angle of cross joint is between 30° and 45°, the rock layers at the slope top slide obviously, and the rock layers near the slope toe bend and uplift sharply, and then the failure develops layer by layer, and finally result in a landslide.

According to the displacement variation curves (see Fig. 9) of the monitoring point *P* at the slope top and the failure characteristics of the slope buckling failure (see Fig.7), the evolution of slope buckling from formation to failure mainly includes three stages. Stage 1 is the initial bending stage, the rock layers move differentially along the dip direction under the action of gravity, and the slope top gradually accelerates to slide downward. There is no space for deformation near the slope toe, and the differential interlayer movement is blocked. The rock layers at the lower part of the slope uplift slightly toward the empty space. Stage 2 is the sharp bending stage. With the continuous action of gravity, the deformation depth and degree of the rock layers in the bending section increase sharply, and the bending uplift continues developing layer by layer until the rock layers are violently bent to the maximum uplift height. Stage 3 is the landslide formation stage. After the buckling of the rock layers in the bending section reaches the maximum height of the buckling, the rock layers below the maximum buckling position begin to collapse, and the resistance of the rock layers above the maximum buckling position gradually decreases, and the sliding speed of the rock layers at the slope top increase fast to form a landslide. The vertical downward sliding displacement at the slope top is about 4.6 m, which is close to the vertical downward sliding displacement of 4.2 m measured in-situ.

According to theoretical calculation, numerical simulation, and field monitoring, the critical buckling length and stability coefficient of the slope are shown in Table 2. From the qualitative analysis, the stability coefficients obtained by the theoretical formulas and the numerical simulation are less than 1, which means that the two methods can predicate the buckling failure of the slop. From the quantitative analysis, when the dip angles of cross joint are 30° and 45°, the critical buckling lengths of the slope obtained by numerical simulation are 13.00 and 11.88 m, respectively. The numerical results are very close to the actual slope buckling length of 12.00 m, while the critical buckling length of the slope obtained by theoretical calculation is 9.42 m, which is slightly less than the actual value. It implies that the results obtained by numerical manifold simulation are more accurate and the theoretical calculation result is slightly conservative. This is because the theoretical formulas are established based on some assumptions, and the slope model is considerably simplified. The rock layers are regarded as ideal elastic continuums, and the influence of cross joints of rock layers is not considered. In the numerical manifold method simulation, interlayer and cross joints are set, and the strength of rock is reduced by considering the geological strength index. Therefore, the numerical simulation calculation model is more consistent with the actual condition, and the results are also similar. In addition, from the data in Table 2, it can also be concluded that the slope buckling failure occurs in the middle and lower parts of the rock layers, which is also in line with the actual situation.

Table 2 Critical bucking length and stability factor of slope

Critical buckling length /m				Stability coefficient λ			
Theoretical value	Numerical solution		Actual value	Theoretical value	Numerical solution		Actual value
	β= 30°	β= 45°			β= 30°	β=45°	
9.42	13.00	11.88	12.00	0.42	0.58	0.53	0.54

7 Conclusion

(1) By presetting interlayer and cross joints, the numerical manifold method can accurately simulate the buckling failure process of layered slope. The buckling deformation and instability failure mode of slope can be shown as: interlayer dislocation − slight bending, slope toe traction−sharp uplift, and accelerated sliding–landslide formation. The formation of landslides is the product of extreme buckling deformation of slopes.

(2) Under the long-term action of self-weight, the evolution of slope buckling from formation to failure mainly includes three stages: initial bending stage, sharp bending stage, and landslide formation stage.

(3) Among the four cross joints with dip angles β of 0°, 15°, 30° and 45°, the slope with 45° cross joint is most prone to slipping and bending deformation, the degree of buckling is the largest, and the number of

time steps of slipping and bending is the least.

(4) When the dip angle of cross joint is between 0° − 15°, the rock layers at the top of the slope slide slightly, but there is no obvious uplift deformation at the lower rock layers. When the dip angle of cross joint is between 30°−45°, prominent buckling deformation of rock layers will occur, and the deformation and failure characteristics can observed to be aligned with the actual situation.

References

[1] HE Qi-biao. Study on stability of No. 2 landslide in front of Lijiaxia hydropower station of Yellow River[J]. Northwest Hydropower, 1992, 26(4): 1−6.

[2] CHEN De-chuan, WANG Jian. Stability study on Bawangshan landslide near Ertan Reservoir[J]. Dam and Safety, 2003(3): 6−9.

[3] SEALE J. An engineering geological investigation of footwall toe-buckle instability at the Malvern Hills opencast coal mine[D]. Christchurch: University of Canterbury; 2006.

[4] SCOBLE M J. Studies of ground deformation in British surface coal mines[D]. Nottingham: University of Nottingham, Mining Engineering Department, 1981.

[5] SUN Guang-zhong. Rock mass structure mechanics[M]. Beijing: Science Press, 1998.

[6] GOODMAN R E. Introduction to rock mechanics[M]. New York: John Wiley and Sons. 1980.

[7] LIU Xiao-li, ZHOU De-pei. Stability analysis of layered dip rocky slopes with elastic plate theory[J]. Rock and Soil Mechanics, 2002, 23(2): 162−165.

[8] ZHU Yu-ping, MO Hai-hou. On critical length of flexural slumping rock layer in layered rocky slope and its influencing factors[J]. Rock and Soil Mechanics, 2004(2): 283−286.

[9] FENG Jun, ZHOU De-pei, YANG Tao. Stability analysis of consequent rock slopes using elastic-plastic plate theory[J]. Chinese Journal of Geotechnical Engineering, 2010, 32(8): 1184−1188.

[10] PAN Rui-lin, LI Bing-sheng, JIANG Jue-guang. Research on the bucking failure of the slab-rent structure rock bedding slopes[J]. Journal of Southwest Jiaotong University, 1990, 77(3): 82−88.

[11] REN Guang-ming, LI Shu-sen, NIE De-xin, et al. The physical simulation and mechanical analysis on landslide's formation mechanism on consequent slope[J]. Mountain Research, 1998, 16(3): 182−187.

[12] TANG Ming-gao, MA Xu, ZHANG Ting-ting, et al. Early recognition and mechanism of creep-bucking of bedding slope[J]. Journal of Engineering Geology, 2016, 24(3): 442−450.

[13] PANT S R, ADHIKARY D P. Implicit and explicit modelling of flexural buckling of foliated rock slopes-technical note[J]. Journal of Rock Mechanics and Geotechnical Engineering, 1999, 32(2): 157−164.

[14] ADHIKARY D P, MÜHLHAUS H B, DYSKIN A V. A numerical study of flexural buckling of foliated rock slopes[J]. International Journal for Numerical and Analytical Methods in Geomechanics, 2001, 25(9): 871−884.

[15] PEREIRA L C, LANA M S. Stress-strain analysis of buckling failure in phyllite slopes[J]. Geotechnical and Geological Engineering, 2013, 31(1): 297−314.

[16] SILVA C, LANA M S. Numerical modeling of buckling failure in a mine slope[J]. Revista Escola de Minas, 2014, 67(1): 81−86.

[17] TOMMASI P, VERRUCCI L, CAMPEDEL P, et al. Buckling of high natural slopes: the case of Lavini di Marco (Trento-Italy)[J]. Engineering Geology, 2009, 109(1-2): 93−108.

[18] SHI Gen-hua. Numerical manifold method and discontinuous deformation analysis[M]. Beijing: Tsinghua University Press, 1997.

[19] ZHANG Guo-xin, PENG Jing. Second-order manifold method in structure failure analysis[J]. Chinese Journal of Theoretical and Applied Mechanics, 2002, 34(2): 261−269.

[20] ZHANG G X. The second order manifold method with six-node triangle mesh[J]. Japan Society of Civil Engineers, 2002, 19(1): 1−9.

[21] ZHANG Guo-xin, ZHAO Yan, SHI Gen-hua, et al. Toppling failure simulation of rock slopes by numerical manifold method[J]. Chinese Journal of Geotechnical Engineering, 2007, 29(6): 800−805.

[22] LIU Hong-yan, WANG Gui-he. Simulation of impact failure of jointed rock mass by numerical manifold method[J]. Rock and Soil Mechanics, 2009, 30(11): 3523−3527.

[23] YANG Shi-kou, REN Xu-hua, ZHANG Ji-xun. Study on hydraulic fracture of gravity dam using the numerical manifold method[J]. Rock and Soil Mechanics, 2018, 39(8): 3055−3060+3070.

[24] HE Jin-fu, WANG Shui-ling. A study on the block-cutting technique of three-dimensional numerical manifold method[J]. Rock and Soil Mechanics, 2020, 41(10): 3473−3480.

[25] YANG Liang, YANG Yong-tao, ZHENG Hong. The phase field numerical manifold method for crack propagation in rock[J]. Rock and Soil Mechanics, 2021, 42(12): 3419−3427.

[26] HOEK E, DIEDERICHS M S. Empirical estimation of rock mass modulus[J]. International Journal of Rock Mechanics and Mining Sciences, 2006, 43(2): 203−215.

[27] HOEK E, BROWN E T. Practical estimates of rock mass strength[J]. International Journal of Rock Mechanics and Mining Sciences, 1997, 34(8): 1165−1186.

[28] HOEK E, CARRANZA-TORRES C, CORKUM B. Hoek-Brown failure criterion[C]//Proceedings of NARMSTac 2002, Mining Innovation and Technology. Toronto: University of Toronto, 2002.

[29] GARZON S E R. Analytical solution for assessing continuum buckling in sedimentary rock slopes based on the tangent-modulus theory[J]. International Journal of Rock Mechanics and Mining Sciences, 2016, 90(10): 53−61.